STRUCTURE OF FLOW FIELDS DOWNSTREAM OF TWO DIFFERENT SWIRL GENERATORS

David Štefan*, Pavel Rudolf*, Sebastian Muntean†, Romeo F. Susan-Resiga‡

This paper discusses the comparison of the flow fields downstream of two different swirl generators. Both swirl generators are used to imitate the flow at the exit of the hydraulic turbine runner and study spatio-temporal behaviour of the swirling flow in the draft tube (i.e. outlet diffuser part of the hydraulic turbine), which undergoes breakdown into vortex rope. Unsteady CFD computations are carried out for identical Reynolds number. Resulting velocity and vorticity profiles are correlated with the structure of the vortex rope. Difference in excited pressure pulsations is illustrated on amplitude-frequency spectra of static wall pressure.

Keywords: *swirl generator, vortex rope, velocity profile, vorticity, pressure fluctuations*

1. Introduction

The control of energy distribution and electricity production are in last several years considerably influenced by electricity produced from renewable sources highly depending on changes in a weather conditions i.e. solar power plants and wind power plants. The pump storage hydro power plants (PSHPP) are proved to be effective to reduce voltage fluctuations in a whole distribution power grid. Control ability of PSHPP is connected with operation of a turbine in extended area, quite far from the best efficiency point (BEP). Unfortunately, operation of the Francis turbine with a constant pitch of the turbine runner (mainly used for PSHPP) at partial discharge, where the flow rate $Q < Q_{\mathrm{BEP}}$, is connected with occurrence of a high swirling flow at the inlet of the draft tube with formation of so called vortex rope. The vortex rope evolution correlates with the vortex breakdown and leads to the high pressure fluctuation in the draft tube. This draft tube surge propagates pressure pulsations into whole machinery system. Moreover, when the frequency of the pressure pulsations generated by the vortex rope rotation corresponds to the natural frequency of machine unit, it can leads to restriction of turbine operation.

In the last decade, these conclusions lead to large investigation of the swirling flow occurred in the Francis turbine draft tube. As a result, FLINDT (Flow Investigation in Draft Tubes) research project was established with a relatively large amount of experimental measured data base describing a wide range of operating points [1, 13]. At last time the experimental data base of the FLINDT project was employed for various theoretical [13, 15, 16],

* Ing. D.,Štefan, doc. Ing. Pavel Rudolf, Ph.D., V. Kaplan Dept. of Fluid Engineering, Faculty of Mechanical Engineering, Brno University of Technology, Technická 2896/2; 61669, Brno, CZ

† Ing. S. Muntean, Ph.D., Centre for Advanced Research in Engineering Sciences, Romanian Academy – Timisoara Branch; Bvd. Mihai Viteazu 24; RO-300223, Timisoara; RO

‡ prof. R. F. Susan-Resiga, Ph.D., Department of Hydraulic Machinery, 'Politehnica' University of Timisoara; Bvd. Mihai Viteazu 1; RO-300222, Timisoara; RO

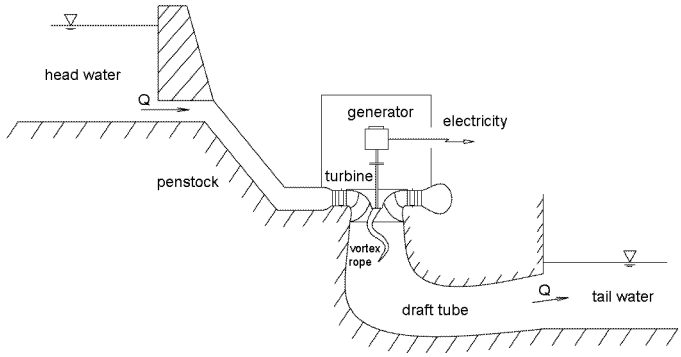

Fig.1: Cross-sectional schema of hydraulic power plant

experimental [6] and computational [5] investigations of the swirling flow. Difficulty of the swirling flow investigation in a scaled model of the hydraulic turbine draft tube leads to an idea of building up a simplified apparatus that best imitates flow at the exit of the hydraulic turbine operated at partial discharge.

2. Swirl generators

The swirl generators have been developed at 'Politehnica' University of Timisoara as well as at V. Kaplan Dept. of Fluid Engineering, Brno University of Technology. The swirl generators are used to study compactness of the generated vortex rope and decay of the vortex rope downstream in the diffuser. Those attributes are further evaluated with the aspect to spectral properties and decrease of the static pressure in the vortex rope with respect to the dynamic pressure at the outlet section of the swirl generator. The particular design of each referred swirl generator is completely different than the other one.

2.1. Swirl generator RO (SG-RO)

The swirl generator SG-RO has been developed by the team at Politehnica University of Timisoara (UPT) and National Center for Engineering Systems with Complex Fluids (NCESCF) as a simplified device to further study the precessing vortex rope [10, 18]. The present swirling flow apparatus consists of four leaned strouts, 13 guide vanes, free runner with 10 blades, convergent divergent draft tube [3, 18] and is mounted into a test rig in hydraulic laboratory at UPT [4]. The stay vanes and the runner vanes were designed using an inverse design technology in order to create the precessing vortex rope [14]. The swirl flow apparatus is also designed to investigate reduction of the pressure fluctuations of the precessing vortex rope by a water injection from the nozzle. For this purpose a water supply is provided by an auxiliary circuit to the leaned shrouds.

The design of SG-RO [18] is such, that the swirl (i.e. axial and circumferential velocity profiles) in a section at the outlet of the runner blades and downstream in the convergent divergent section is similar to the Francis turbine investigated by Ciocan et al. [5].

The numerical simulation of the convergent divergent section was carried out by Muntean et al. [9] and Petit et al. [10]. Both commercial software ANSYS Fluent and open source software OpenFOAM were employed to compute the unsteady swirling flow with the precessing vortex rope in order to compare numerical results provided by software codes and

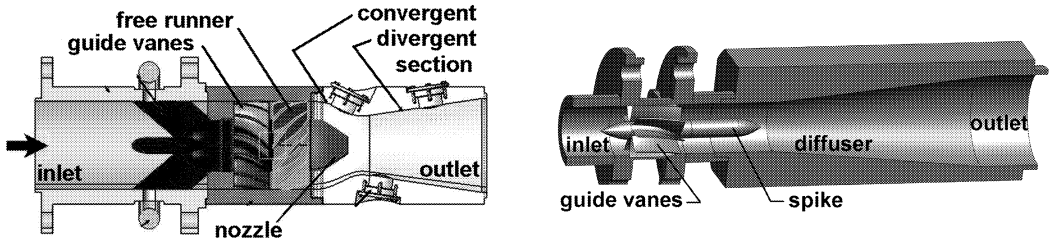

Fig.2: Experimental setup of swirl generators SG-RO on the left and SG-CZ on the right

experimental results. Due to lower computational requirements the realizable k-ε turbulence model was applied.

2.2. Swirl generator CZ (SG-CZ)

Differently designed swirl generator has been developed at V. Kaplan Dept. of Fluid Engineering, Faculty of Mechanical Engineering, Brno University of Technology. The swirl generator consists of 10 fixed blades with relatively long narrow channels to prevent flow separations along the blade surface for a broad range of operating regimes. CFD simulation proved that almost identical velocity angles are provided by the generator for flow rates between 4 and 13 l/s [12]. The swirl generator is part of the test rig placed in hydraulic laboratory of V. K. Dept. of Fluid Engineering. The test rig is supplied from a tank by a centrifugal pump and the swirl generator is situated approximately in the middle of pipeline system. Control of the discharge is enabled via frequency convertor coupled to the centrifugal pump.

3. Swirling flow

The swirling flow in diffusers is a subject of investigation because of the phenomena (e.g. vortex breakdown, vortex rope), which are not still completely described and understood. A summary of the vortex breakdown research can be found in Luca-Negro et al. [8], where significant influences on the vortex rope formation are described.

The experimental and numerical results show, that a shape of the circumferential velocity profile, namely location of the velocity maximum and magnitude of the maximum velocity are decisive for the shape of the cavitating vortical structure [12]. It has to be pointed out, that the two structurally diverse swirl generators produce completely different structure of the vortex ropes.

4. CFD calculation

In order to compare the swirling flows generated by each swirl generator and the resulting vortex rope developing in downstream parts, the unsteady computation is carried out by a commercial software ANSYS Fluent R13 using a Reynolds Averaged Navier-Stokes equations (RANS) and a Linear Pressure-strain Reynolds-stress turbulence model (RSM) for turbulence modeling. The near-wall treatment was set to the Non-equilibrium wall functions. The considered computational domains are downstream parts of the swirl generator apparatuses and diffusers. For a better comparison of computed results, we employed the RSM turbulence model with higher computational requirements but better performance for

the highly swirling flows [7]. The effect of a strong turbulence anisotropy can by modeled rigorously only by the second-moment closure adopted in the RSM [16].

Both computational domains include mesh with approximately 2 million hexahedral cells. The velocity components, the turbulence kinetic energy k and the rate of turbulence dissipation ε, obtained from the separate computation of the blade part of the swirl generator, are defined as the inlet boundary conditions. At the outlet boundary condition the radial equilibrium distribution of the static pressure, where the pressure gradient is governed by the radial component of the Euler equation (1).

$$\frac{\partial p}{\partial r} = \frac{\varrho\, v_\theta^2}{r} \tag{1}$$

where r is a distance from the axis of a rotation and v_θ is a circumferential velocity. At the centre of the boundary the value of the static pressure is set to 0 Pa. The mesh quality is presented by a dimensionless distance from the wall defined as

$$y^+ = \frac{u_\tau\, y}{v} \tag{2}$$

where $u_\tau = \sqrt{\tau_\mathrm{w}/\varrho}$ is a friction velocity, y is a normal distance from the wall and τ_w is a wall shear stress. By general rule the magnitude of y^+ is recommended in interval $y^+ \in (30; 120)$ in order to obtain suitable results.

4.1. Computational domain of downstream part of SG-RO

In case of the SG-RO the computational domain CD-RO is convergent divergent section with the inlet diameter 150 mm, the throat diameter $D = 100$ mm and the outlet diameter 160 mm. The survey section S_0 is situated in the throat as a boundary between the convergent and the divergent section. The survey sections S1, S2 and S3 are in distances $0.5\,D$, D and $1.5\,D$ from the S_0. The longitudinal cross section of the CD-RO with position of the survey sections is shown in fig. 3. The magnitude of y^+ (2) in most of area of the SG-RO computational domain lies in interval $y^+ \in (40; 100)$.

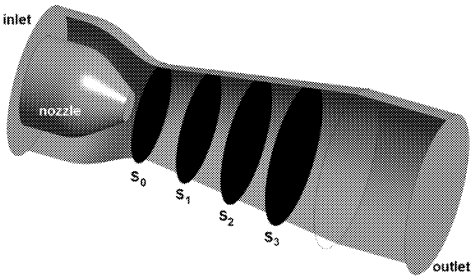

Fig.3: Computational domain (CD-RO) in case of SG-RO

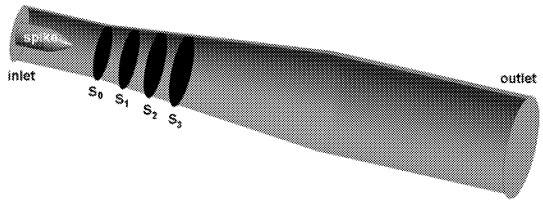

Fig.4: Computational domain (CD-CZ) in case of SG-CZ

4.2. Computational domain of downstream part of SG-CZ

The computational domain CD-CZ as a downstream part of the SG-CZ is a diffuser with the inlet diameter 53.6 mm, the outlet diameter 98 mm and the opening angle 12°.

The survey section S0 is placed at the end of the cylindrical part with a same diameter as the inlet diameter $D = 53.6\,\text{mm}$. The survey sections S_1, S_2 and S_3 are in distances $0.5\,D$, D and $1.5\,D$ from the S_0. The longitudinal cross section of CD-RO with position of survey sections is shown in fig. 4. The magnitude of y^+ (2) in most of area of the SG-CZ computational domain lies in interval $y^+ \in (15; 40)$.

4.3. Computational set-up

The numerical computations were carried out for flow regimes with the identical Reynolds number Re

$$Re = \frac{\bar{v}\,D}{v} \tag{3}$$

defined in the survey section S_0. The value of Reynolds number is $Re = 380143$ and corresponds to the flow rate $Q = 30\,\text{l/s}$ for SG-RO and $Q = 15.9\,\text{l/s}$ for SG-CZ. In fig. 5 are shown velocity profiles generated by the SG-RO and in fig. 6 profiles generated by the SG-CZ. Those profiles were used as the inlet boundary conditions for numerical computations. Only the axial and circumferential components are shown because of very small magnitude of the radial velocity component. But in the boundary condition the radial component is included. The velocity components are circumferentially averaged and made dimensionless with respect to the bulk velocity at the outlet of the swirl generator.

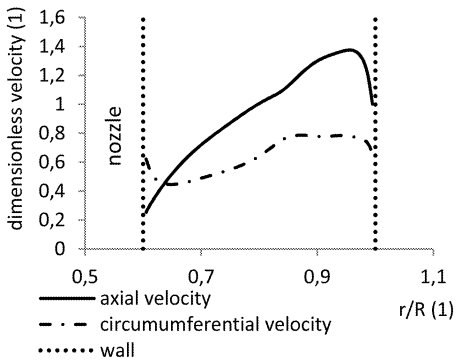

Fig.5: Velocity components generated by SG-RO

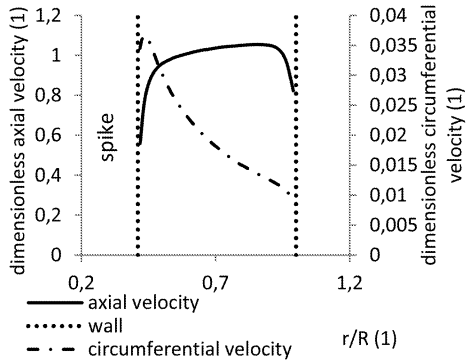

Fig.6: Velocity components generated by SG-CZ

5. Evaluation and results

For a global quantitative description of the swirling flow we used the swirl number S_n

$$S_\text{n} = \frac{\int v_\text{ax}\, v_\text{tan}\, r\, \text{d}S}{R \int v_\text{ax}^2\, \text{d}S} \tag{4}$$

defined as the axial flux of the swirl momentum divided by the axial flux of the axial momentum [13, 17]. Computed value of the swirl number generated by the SG-RO is $S_\text{n-RO} = 0.581$ and is substantially larger than the swirl number computed in case of the SG-CZ where $S_\text{n-CZ} = 0.122$. The evolution of the swirl number (4) along the diffuser length is plotted in fig. 7. This difference is also noticeable in dimensionless circumferential velocity components, see fig. 5 and fig. 6. The comparison for the identical swirl number is not carried out due

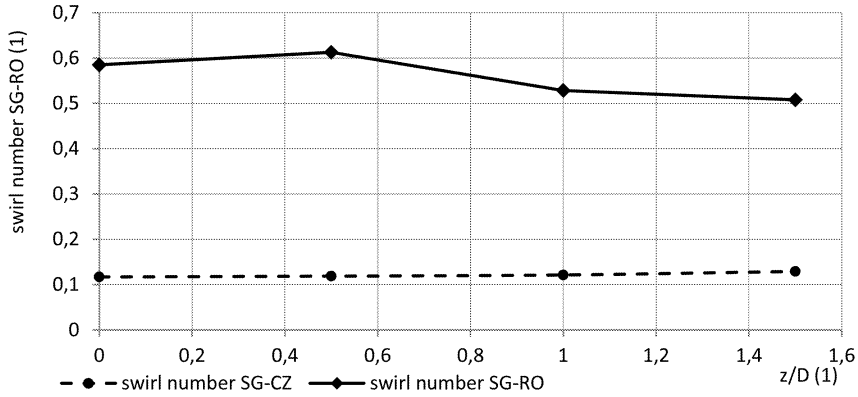

Fig.7: Swirl number streamwise development in case of CD-RO (solid line) and CD-CZ (dashed line)

to a different design of the swirl generators (blade design of SG-CZ produces much smaller circumferential velocity component than SG-RO).

5.1. Velocity profiles computed in the survey section S_0

The velocity profiles computed in the survey sections S_0 are time averaged and made dimensionless with respect to the equation (5).

$$v_{\text{dim-less}} = \frac{v}{\frac{Q}{S}} = \frac{v}{\bar{v}} \tag{5}$$

where v is a corresponding velocity component and $\bar{v}$ is a bulk velocity defined as a flow rate Q divided by a cross-sectional area S.

The dimensionless axial velocity components (fig. 8) and the circumferential velocity components (fig. 9) computed in a survey section of the corresponding swirl generator are plotted against the dimensional radial coordinate.

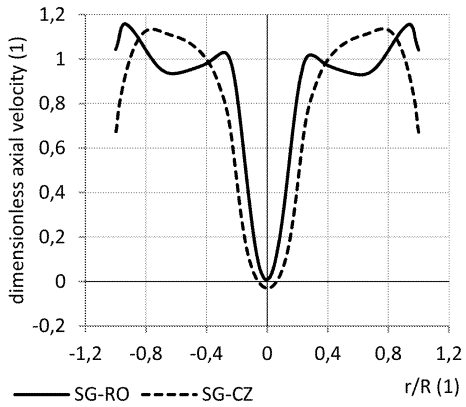

Fig.8: Dimensionless axial velocity components computed in survey section S_0

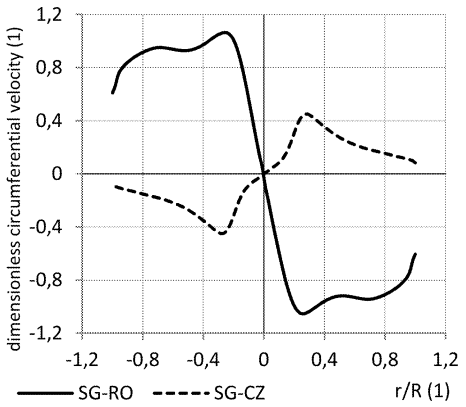

Fig.9: Dimensionless circumferential velocity components computed in survey section S_0

5.2. Streamwise evolution of axial velocity, circumferential velocity and vorticity magnitude

The evolution of axial velocity components along the diffuser axis are shown in figs. 10 and 13. The enlargement of the stagnant region is evident and related with extending of the vortex rope helix in the streamwise direction. The axial velocity component is much larger in case of the SG-CZ than in case of the SG-RO. On the other hand the circumferential velocity component is much smaller in case of the SG-CZ than in case of the SG-RO. A different sense of the flow rotation, caused by a different design of the swirl generators, is noticeable in the circumferential velocity profiles (see fig. 11 versus fig. 14 or fig. 9). Magnitudes of corresponding profiles (axial, circumferential or vorticity) are plotted in an equal dimensional scale.

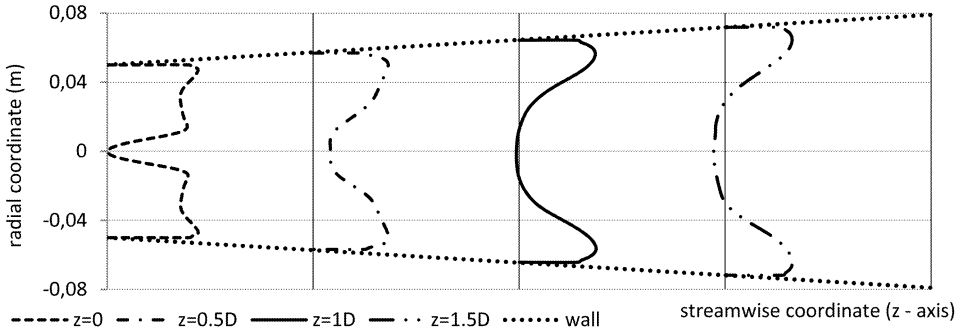

Fig.10: Time averaged axial velocity profile development downstream in diffuser of CD-RO

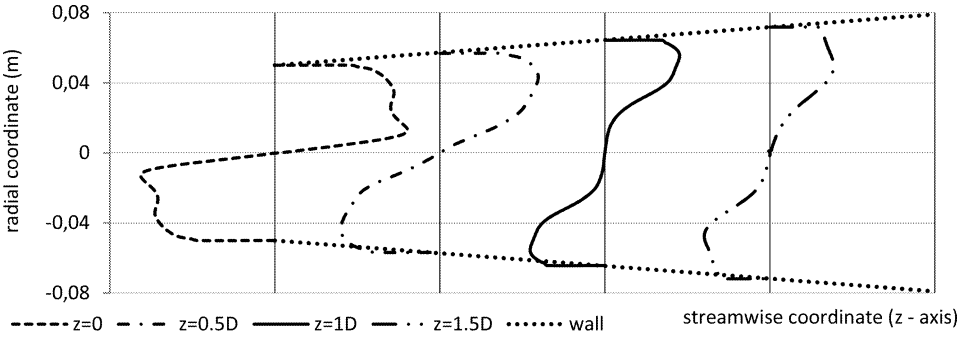

Fig.11: Time averaged circumferential velocity profile development downstream in diffuser of CD-RO

An important fact is, that boundary of the stagnant region (apparent by the large gradient of the velocity profile curve), lies in an appropriate distance from the diffuser axis for both, axial and circumferential velocity component. This fact shows a strong coupling between corresponding axial and circumferential velocities [2].

The vorticity magnitude profiles evolution (fig. 12 versus fig. 15) shows a higher compactness of the vortex core in a streamwise direction (significant peaks of vorticity) for case of SG-CZ. This conclusion is evident in fig. 17, where streamlines wind around the vortex rope keep a helical shape along the diffuser. The abrupt vortex decay, approximately situated

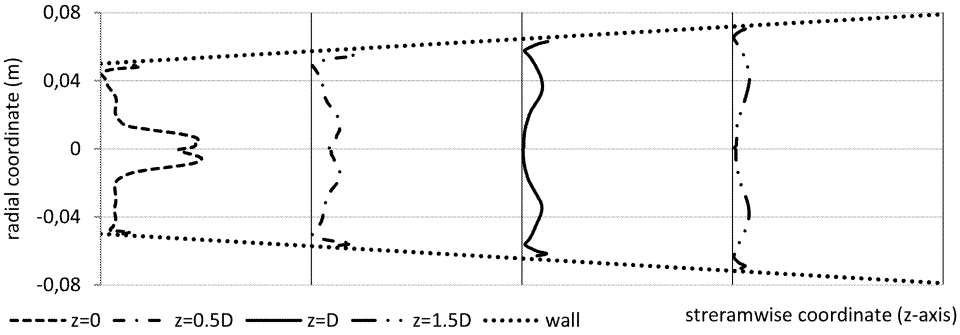

Fig.12: Time averaged vorticity magnitude profile development downstream in diffuser of CD-RO

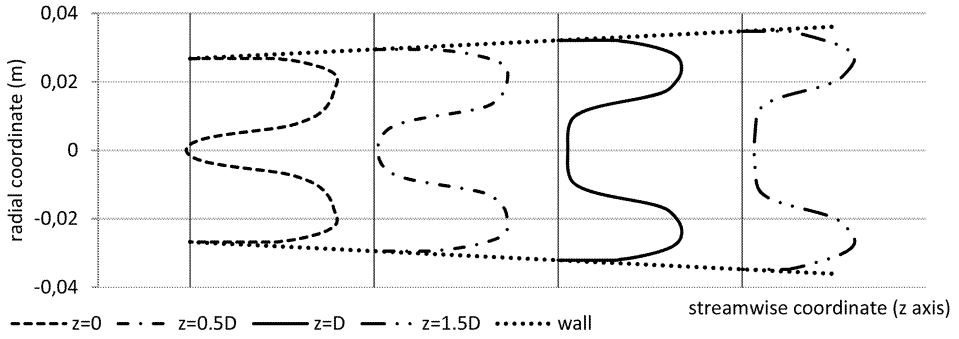

Fig.13: Time averaged axial velocity profile development downstream in diffuser of CD-CZ

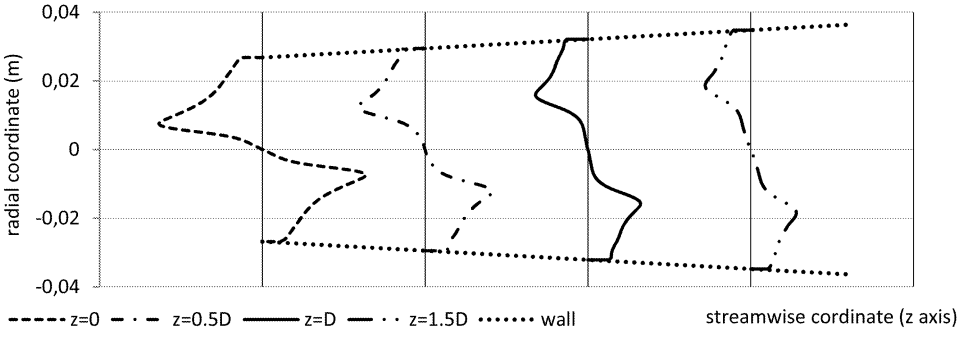

Fig.14: Time averaged circumferential velocity profile development downstream in diffuser of CD-CZ

near the survey section S_1, is apparent in case of the SG-RO. This abrupt vortex decay is also probably related with a formation of the huge backflow region (visualized in fig. 17 (left) as a time averaged) and linked with the significant longitudinal vortex rope pulsation with a computed frequency around 2.5 Hz (see figs. 22 and 23).

5.3. Flow field analysis

The calculation is based on a one phase model, thus for the vortex rope visualization is applied an isosurface of very low pressure. The significant difference is noticeable between

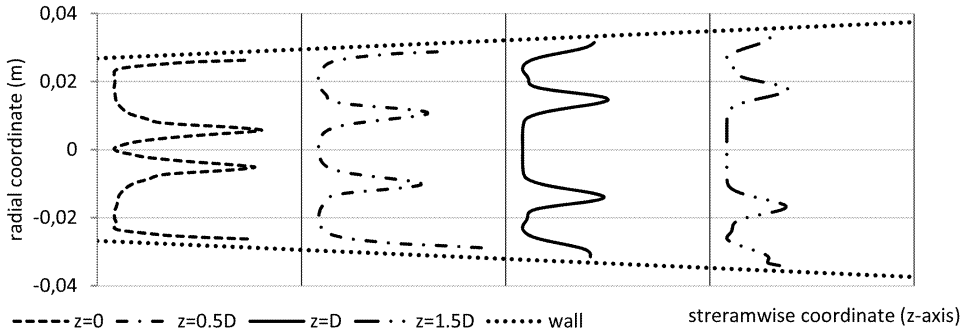

Fig.15: Time averaged vorticity magnitude profile development downstream in diffuser of CD-CZ

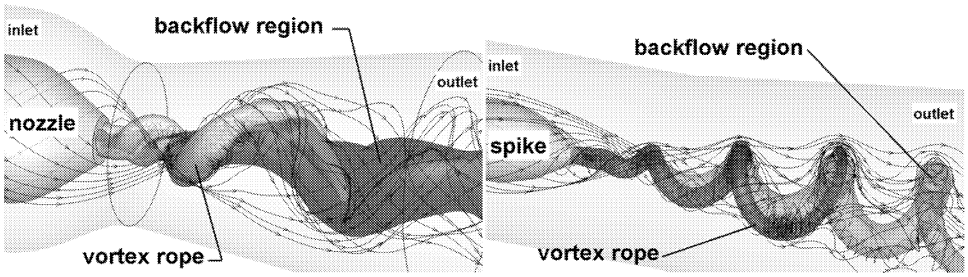

Fig.16: Vortex rope and instantaneous snapshot of backflow region, CD-RO on the left and CD-CZ on the right

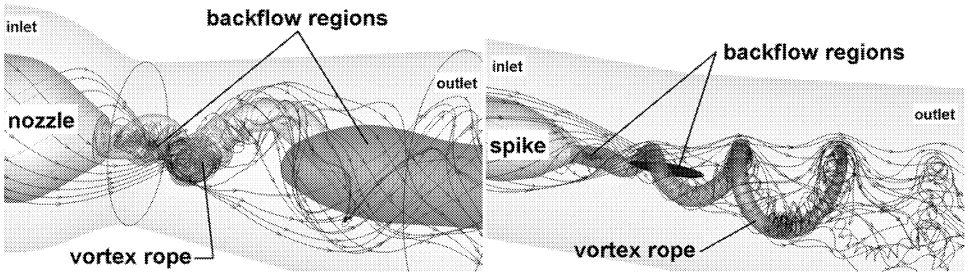

Fig.17: Vortex rope and time averaged backflow regions, CD-RO on the left and CD-CZ on the right

pressure drop generated by each swirl generator. The vortex ropes are visualized for a ratio $p_{\mathrm{stat}}/p_{\mathrm{dyn\_inlet}} = -1.95$ in case of the SG-RO and -1.08 in case of the SG-CZ, where p_{stat} is a value of static pressure isosurface and $p_{\mathrm{dyn\_inlet}}$ is a dynamic pressure at the inlet of the computational domain. The time snapshot of the vortex ropes with instantaneous backflow regions are shown in fig. 16. On the other hand the time averaged backflow regions are visualized in fig. 17.

5.3.1. Time development of SG-RO vortex rope

Time-instability of the vortex rope generated by the SG-RO is sufficiently visualized by the time-snapshots in fig. 18. Longitudinal extension and reduction of the vortex rope is also related with the significant pressure pulsations, so called synchronous pressure pulsa-

tions. Character of these pulsations can be extracted from the time signal of computed static pressure in two oppositely oriented monitoring points 'mg0 +y axis' (solid line) and 'mg0 −y axis' (dashed line) each other rotated by 90 degrees. These time signals are plotted in the middle of fig. 18 and corresponding snapshots are assigned by arrows. Each of time signals is evidently compounded from two sinusoidal waves, where the wave with the longer time period and same phase for both monitoring points corresponds to the longitudinal instability of the vortex rope. This time period is around 0.4 s and corresponds to frequency around 2.5 Hz extracted from the pressure signal evaluated in the section 5.4. A transition from one long vortex rope ($t = 0$ s) to one longer and one very short intertwined vortex ropes ($t = 0.1$ s or 0.2 s) is noticeable. On the other hand so called asynchronous pressure pulsations with the frequency around 14.95 Hz and opposite phase are related with the rotational movement of the vortex rope.

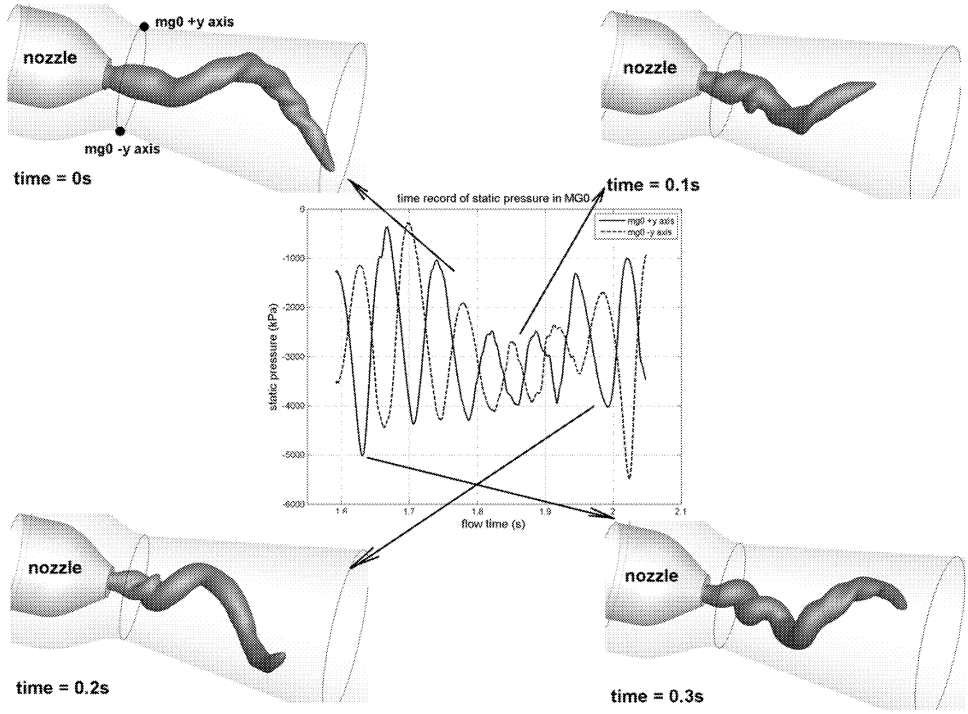

Fig.18: Longitudinal development of SG-RO vortex rope in time

5.3.2. Comparison with experimental measurement

In this section the axial and the circumferential velocity components extracted from the CFD computation are compared with the experimentally measured velocity components carried out by 2D LDV measurement in case of the SG-RO [4], see fig. 19. Comparison is carried out for two survey sections corresponding with window W1 (plotted in fig. 20) and window W2 (plotted in fig. 21). One can see good fitting of numerical curves with the experimentally measured axial velocity. A higher discrepancy appears in circumferential velocity component outside of the diffuser axis, where the computed circumferential velocity profiles are flatter than the measured ones.

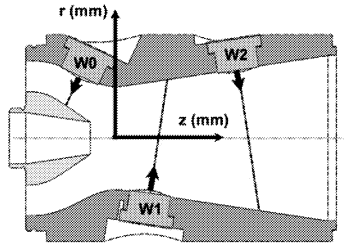

Fig.19: Survey axis for LDV measurement in convergent divergent part of SG-RO [4]

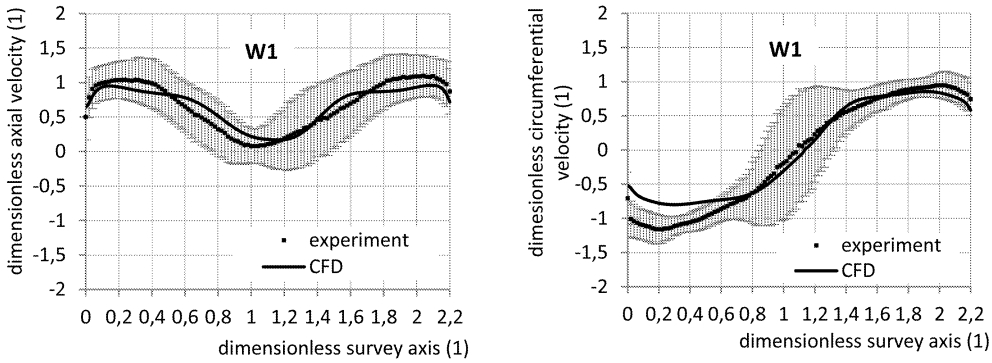

Fig.20: Velocity components from 2D LDV measurement compared with CFD results (window W1)

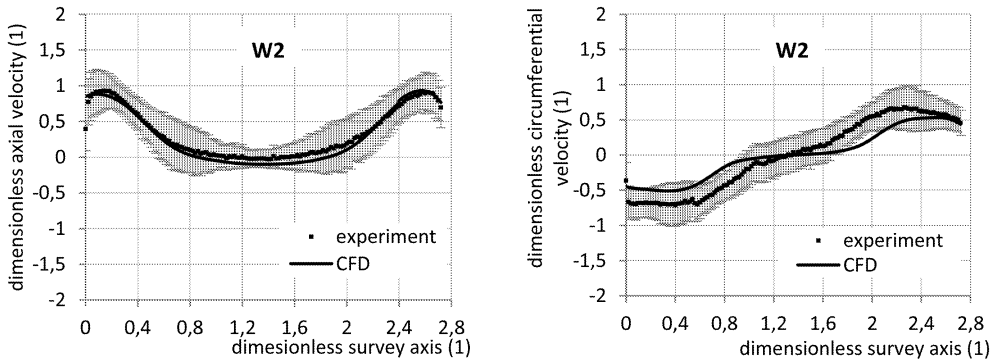

Fig.21: Velocity components from 2D LDV measurement compared with CFD results (window W2)

5.4. Fourier analysis of the pressure fluctuations

As results of the vortex breakdown the high pressure fluctuations are generated in a downstream part of the swirl generator. The time record of numerically computed static pressure was set in four monitoring points to perform the Fast Fourier Analysis. The monitoring points are situated near the wall of the computational domain in downstream distances in order 0, 0.5 D, D and 1.5 D from the S_0, where D is a diameter of the survey section S_0. The simple script written in MATLAB software was employed to extract the spectral information

of the numerical pressure record. The frequencies with dominant amplitudes are shown in tab. 1 for CD-RO and in tab. 2 for CD-CZ. Amplitudes related to the inlet dynamic pressure p_{dyn} are written in fourth column of the tables.

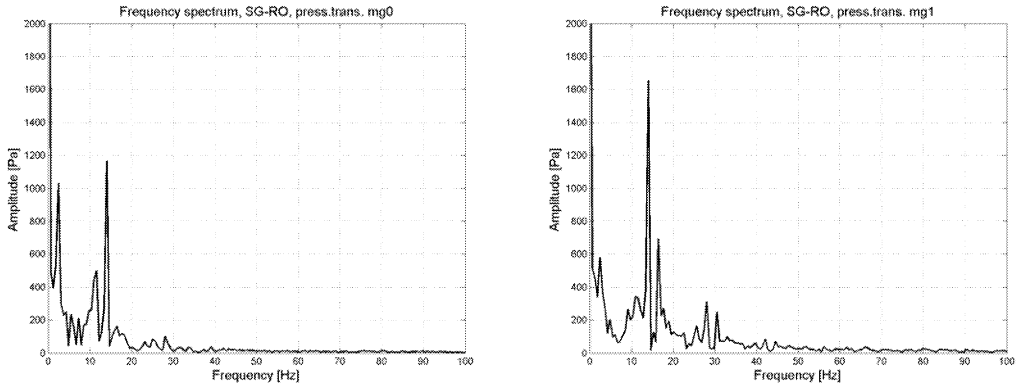

Fig.22: Amplitude-frequency spectrum of pressure pulsations in case of CD-RO (MG0 on the left, MG1 on the right)

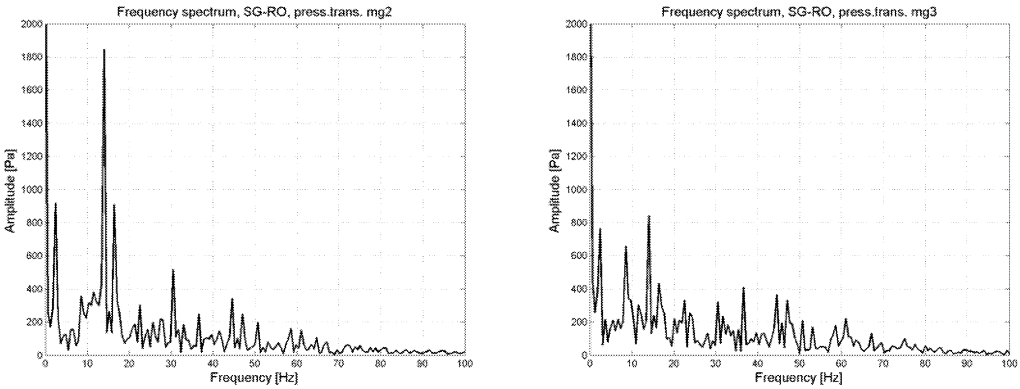

Fig.23: Amplitude-frequency spectrum of pressure pulsations in case of CD-RO (MG2 on the left, MG3 on the right)

Monitoring point	Dominant frequency (Hz)	Amplitude (Pa)	Amplitude/p_{dyn} (1)
MG0	14.04	1166	0.189
MG1	14.04	1655	0.268
MG2	14.04	1847	0.299
MG3	14.04	843	0.137

Tab.1: Spectral analysis of CD-RO

Monitoring point	Dominant frequency (Hz)	Amplitude (Pa)	Amplitude/p_{dyn} (1)
MG0	99.46	172.5	3.37×10^{-3}
MG1	99.46	189.9	5.02×10^{-3}
MG2	99.46	191	5.04×10^{-3}
MG3	99.46	237.4	6.28×10^{-3}

Tab.2: Spectral analysis of CD-CZ

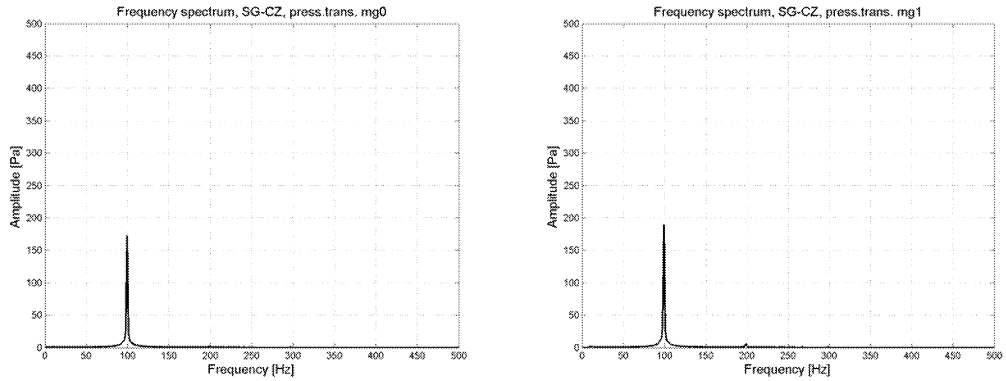

Fig.24: Amplitude-frequency spectrum of pressure pulsations in case of CD-CZ (MG0 on the left, MG1 on the right)

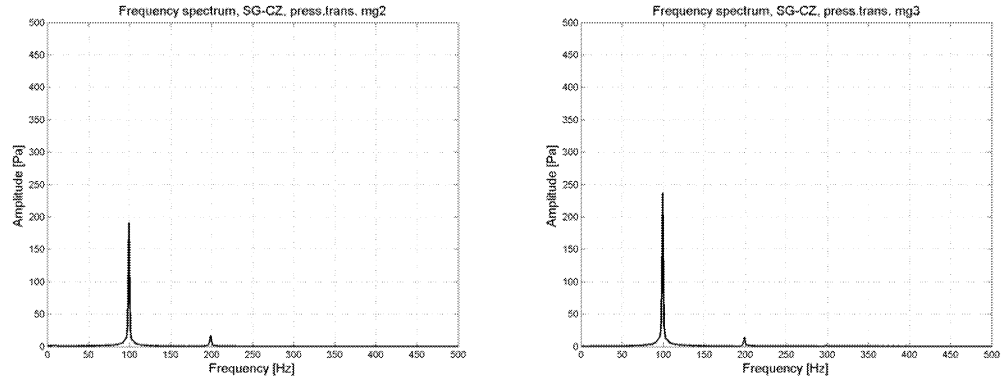

Fig.25: Amplitude-frequency spectrum of pressure pulsations in case of CD-RO (MG2 on the left, MG3 on the right)

5.4.1. Comparison with experimental measurement

The experimentally measured frequency of the vortex rope rotation in case of the SG-RO is found around 14.95 Hz. One can see only small difference (6 %) between the experimentally measured and the numerically computed frequencies and good agreement with a previously computed results [9, 10]. The lower value of the numerical frequency confirms that the numerical model is more dissipative than the experiment. Suitable agreement in comparison of numerical and experimental [9] amplitude magnitude is obtained only for the pressure transducers MG0, while the computed amplitudes for MG1, MG2 and MG3 overestimate experimental results. The comparison for case of SG-CZ is not carried out because of high interference in experimental data. This problem is being further investigated.

6. Conclusions

A different shape of the vortex rope, generated by each swirl generator, corresponds to a different value of the swirl number. The SG-RO with the higher swirl number than the SG-CZ composes swirling flow with a more massive vortex rope. The vortex rope has larger

width and forms into shape with a higher ascend of the helix. This shape is similar to the vortex rope appearing in the Francis turbine draft tube (FLINDT project) during operation on 70 % Q_{BEP} and was main designed parameter of the SG-RO.

On the other hand, the vortex rope generated by the SG-CZ is thinner and forms into shape with a lower ascend of the helix. In a comparison with the vortex ropes computed in paper [11] for inlet boundary conditions derived by Susan-Resiga et al. [13], the vortex rope generated by the SG-CZ is very similar one to the vortex rope corresponding with the turbine operation on 90 % Q_{BEP}.

The calculated shape of the vortex rope generated by the SG-RO is more unstable than the vortex rope generated by the SG-CZ. Moreover for a calculation employing the RSM turbulence model, the vortex rope changes its structure periodically from one long compact vortex rope into two (long and one very short) vortex ropes which are intertwined close to the nozzle. This change realized in the longitudinal direction is a result of the synchronous pressure pulsations with the frequency around 2.5 Hz and the amplitude around 800 Pa.

Presented results also confirmed strong coupling between the circumferential and the axial velocity components and this coupling is full maintained in the streamwise direction.

Acknowledgement

Czech Science Foundation is gratefully acknowledged for support of the research under project No. 101/09/1715 'Cavitating vortical structures induced by rotating liquid'. This project is supported by junior research grant number FSI-J-13-2019 provided by Brno University of Technology. The Timisoara swirl generator test case and associated experimental data was supported by the Romanian Agency CNCSIS – UEFISCSU, Exploratory Research Project PN II – IDEI 799/2008.

References

[1] Avellan F.: Flow Investigation in a Francis Draft Tube: The FLINDT Project, in: Proceedings of the 20$^{\mathrm{th}}$ IAHR Symposium on Hydraulic Machinery and Systems, Charlotte, USA 2000, Paper DES-11

[2] Batchelor G.K.: Axial Flow in Trailing Line Vortices, J. Fluid Mech. 20 (4) (1964), pp. 645–658

[3] Bosioc A., Susan-Resiga R.F., Muntean S.: Design and Manufacturing of a Convergent-Divergent Test Section for Swirling Flow Apparatus, in: Proceedings of the 4$^{\mathrm{th}}$ German – Romanian Workshop on Turbomachinery Hydrodynamics (GRoWTH), June 12–15, Stuttgart 2008, Germany

[4] Bosioc A., Tanasa C., Muntean S., Susan-Resiga R.F.: 2D LDV Measurements of Swirling Flow in a Simplified Draft Tube, in: Proceedings of the CMFF09, Vol. II, Budapest 2009, Hungary, p.p. 833–838

[5] Ciocan G. D., Iliescu M.S., Vu T.C., Nennemann B., Avellan F.: Experimental study and numerical simulation of the FLINDT draft tube rotating vortex, Journal of Fluids Engineering, Vol. 129 (2007), pp. 146–158

[6] Iliescu M. S., Ciocan G.D., Avellan F.: Analysis of the Cavitating Draft Tube Vortex in a Francis Turbine Using Particle Image Velocimetry Measurements in Two-Phase Flow, Journal of Fluid Engineering, Vol. 130 (2008)

[7] Jawarneh A.M., Vatistas G.H.: Reynolds Stress Model in the Prediction of Confined Turbulent Swirling Flows, in: ASME Journal of Fluid Engineering, Vol. 128 (2006), p.p. 1377–1382

[8] Lucca-Negro O., O'Doherty T.: Vortex breakdown: a review, in: Annual Review of Fluid Mechanics, 10 (2001), 221–246

[9] Muntean S., Nilsson H., Susan-Resiga R.: 3D Numerical Analysis of the Unsteady Turbulent Swirling Flow in a Conical Diffuser Using Fluent and OpenFOAM, in: Proceedings of the 3rd IAHR International Meeting of the Workgroup on Cavitation and Dynamic Problem in Hydraulic Machinery and Systems, Brno 2009, Czech Republic

[10] Petit O., Bosioc A.I., Nilsson H., Muntean S., Susan-Resiga R.F.: Unsteady Simulations of the Flow in a Swirl Generator, Using OpenFOAM, International Journal of Fluid Machinery and Sytsems, Vol. 4, No. 1 (2011)

[11] Rudolf P.: Connection between inlet velocity field and diffuser flow instability, in: Applied and Computational Mechanics, Vol. 3, No. 1 (2009), pp. 177–184

[12] Rudolf P., Hudec M., Zubík P., Štefan D.: Experimental measurement and numerical modeling of cavitating flow in converging-diverging nozzle, in: Proceedings of the International Conference Experimental Fluid Mechanics, pp. 423–431, Jíčín 2011, Czech Republic

[13] Susan-Resiga R.F., Ciocan G.D., Anton I., Avellan F.: Analysis of the swirling flow downstream of a Francis turbine runner. Journal of Fluid Engineering, Vol. 128 (2006), pp. 177–189

[14] Susan-Resiga R.F., Muntean S., Bosioc A.: Blade Design for Swirling Flow Generator, in: Proceedings of the 4th German – Romanian Workshop on Turbomachinery Hydrodynamics (GRoWTH), June 12–15, Stuttgart 2008, Germany

[15] Susan-Resiga R.F., Muntean S., Avellan F., Anton I.: Mathematical modelling of swirling flow in hydraulic turbines for the full operating range, Appl. Math. Modell (2011), doi:10.1016/j.apm.2011.03.052

[16] Susan-Resiga R.F., Muntean S., Hasmatuchi V., Anton I., Avellan F.: Analysis and prevention of vortex breakdown in the simplified discharge cone of a Francis turbine, Journal of Fluid Engineering, Vol. 132 (2010), 15 pages

[17] Susan-Resiga R.F., Muntean S., Stein P., Avellan F.: Axisymmetric swirling flow simulation of the draft tube vortex in Francis turbines at partial discharge, in: Int. J. Fluid Mach. Sys. 2 (2009), pp. 295–302

[18] Susan-Resiga R.F., Muntean S., Tanasa C., Bosioc A.: Hydrodynamic Design and Analysis of a Swirling Flow Generator, in: Proceedings of the 4th German – Romanian Workshop on Turbomachinery Hydrodynamics (GRoWTH), June 12–15, Stuttgart 2008, Germany

Received in editor's office: January 13, 2013
Approved for publishing: April 2, 2013